Simulation of Polyester Melt Spinning with Axial Quench for Increasing Productivity

P.T. Sumesh,* T.P. Mathur,† U.S. Agarwal

Reliance Technology Group, Reliance Industries Limited, B-4 MIDC Industrial Area, Patalganga 410220, Dist. Raigad, Maharashtra, India

Received 7 April 2009; accepted 26 October 2009
DOI 10.1002/app.31710
Published online 20 January 2010 in Wiley InterScience (www.interscience.wiley.com).

ABSTRACT: Production of polyester filament involves melt spinning into partially oriented yarn (POY), followed by drawing to enhance the bulk and mechanical properties. The industrial demand of increasing productivity is generally met by increasing POY melt spinning speeds, which is limited by increasing polymer chain orientation (and reducing residual drawability) in the POY produced at higher spinning speeds. Modification of the quench geometry during melt spinning is claimed to allow reduction of air drag and polymer chain orientation, permitting an increase in productivity during melt spinning into POY. We present a simple way for modeling the quenching of molten filaments under the modified (axial) air flow. Numerical simulations of the melt spinning are developed to demonstrate the influence of the quench geometry modification as we compare the process with the conventional cross-flow quench and the modified axial quench. We find that increasing quench air flow reduces the polymer chain orientation, in contrast to the well known effect in cross-flow quench.
© 2010 Wiley Periodicals, Inc. J Appl Polym Sci 116: 2541–2547, 2010

Key words: melt spinning; axial air flow; drag reduction; delayed quenching

INTRODUCTION

One of the most widely used industrial process for the production of polymeric/non-polymeric fibers is melt spinning. This involves extrusion of the polymer melt through small capillary hole, cooling with air flowing across the spinline while being drawn due to winding of the solidified filaments at high speed. In the particular case of polyester [polyethylene terephthalate (PET)] filament produced at winding speeds of 2500–3500 m/min, the filament produced are partially oriented yarn (POY), and are then subjected to further processes of thermomechanical drawing for improving the physical properties. The constant industrial demand of increased productivity of polymeric fibers from given melt spinning hardware is generally met by increased take-up speeds during the melt spinning process. However, the extent of such increase is limited, as the increasing take-up speeds increase the strain rates in the spinline and the polymer chain orientation (and orientation induced crystallization) and decrease the residual drawability of the as-spun filament as well as the productivity of the subsequent drawing process.[1] Several approaches have been reported towards overcoming this limitation, and include crystallization suppression by branching,[2–4] blending with small amount of immiscible polymer[5–10] copolymerization,[11] delayed quenching, etc to suppress orientation and/or crystallization. A more recent innovation to overcome this difficulty is modification of quench air flow to impart axial velocity along the filament movement, thereby reducing the drag force and slowing the stress induced crystallization.[12,13]

Polymer melt spinning involves complex interactions of mass, momentum and heat transport governing processes, and associated polymer melt rheological behavior and the structural development through glass transition, polymer chain orientation and orientation induced crystallization. Modeling and simulation of polymer melt spinning incorporating these phenomena has greatly helped enhance the understanding of the cross-flow quenched melt spinning process of polymers, such as polyester, emerging in near quantitative prediction of the effects of process parameters, such as melt temperature and viscosity, melt flow rate, quench air speed and temperature, take-up speed, etc.[14] A similar understanding in the case of melt spinning with axial air flow is lacking, even as it differs dramatically from the cross-flow quenched melt spinning. For example, while spinline stress during melt spinning increases with increasing quench air flow with cross flow of

**Present address:* Engineering Mechanics Unit, Jawaharlal Nehru Centre for Advanced Scientific Research, Jakkur, Bangalore – 560064, India.
†*Present address:* G10, Sree One Paradise, 5th Cross, Lakshmi Layout, Munnekolala, Marathalli, Bangalore – 560037, India.
Correspondence to: U.S. Agarwal (uday.agarwal@ril.com).

© 2010 Wiley Periodicals, Inc.

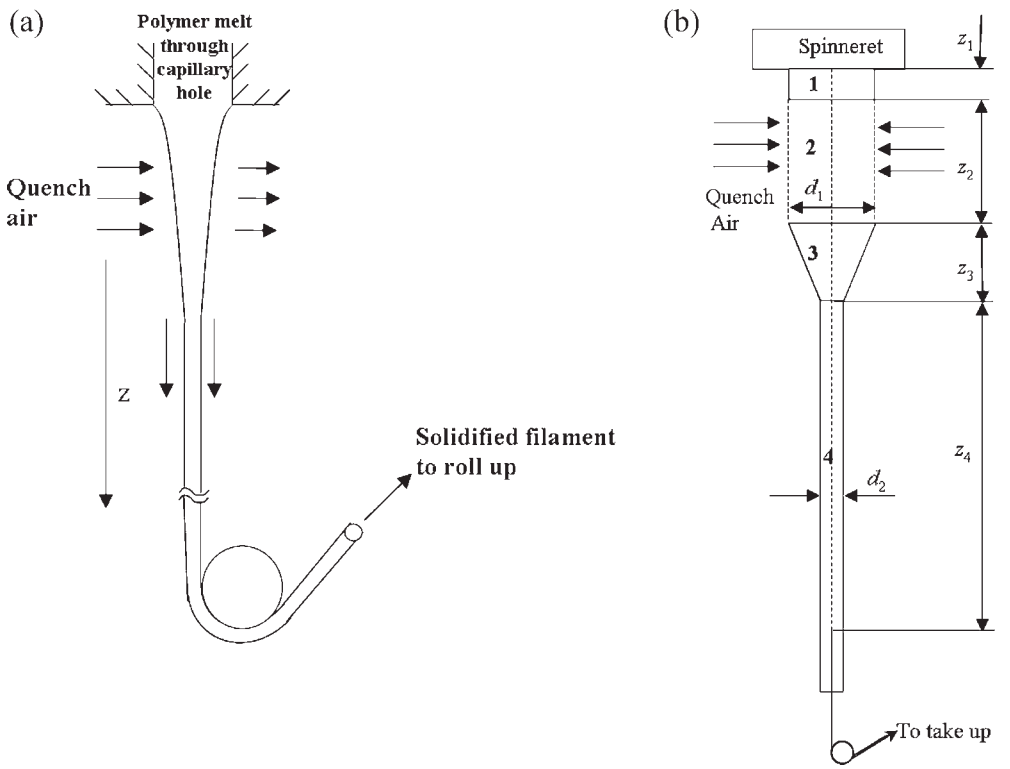

Figure 1 (a) Schematic diagram of a single filament melt spinning with cross-flow quench (b) Schematic of melt spinning with axial quench. A tube composed of the following four sections is used to manipulate the air flow field around the filament, section 1 – quench delay ($d_1 = 95$ mm, $z_1 = 50$ mm), section 2 – air inlet ($z_2 = 190$ mm), section 3 – accelerating region ($z_3 = 125$ mm), Section 4– long tube of constant cross-section ($z_4 = 425$ mm, $d_2 = 26$ mm).

air, the same is not true with axial-flow quench. In this article, we present an extension of the cross-flow quenched melt spinning models to allow us a simplistic treatment of the axial-flow quench melt spinning. The model is then used to simulate effect of various parameters.

THE MELT SPINNING PROCESS

A typical process of melt spinning is shown in [Fig. 1(a)]. Polymer is heated above its melting temperature, fine filtered, and extruded through capillary hole(s) of a spinneret. This molten polymer is quenched by cold air while being drawn to take-up rolls, running at very high speeds, called the take-up speed. The polymer melt starting from the spinneret towards the take-up roller experiences increasing velocity, and decreasing temperature and filament diameter, as well as the corresponding variation in strain rate and rheological stress at positions along the spinline until reaching the freeze point corresponding to glass transition temperature (T_g) of the polymer. The stress at the freezing point plays a decisive role of determining in the final properties of the filament, the freeze-point stress being directly related to the level or molecular orientation and tenacity, and inversely related to the residual elongation of the solidified POY.

MODELING THE MELT SPINNING PROCESS

We use a standard model[14] available in the literature to describe the process of melt spinning. It incorporates the mass, momentum, and energy conservation laws of the polymer melt of a single filament [eqs. (1)–(4)].

$$W = \rho A \nu \tag{1}$$

$$\frac{dF}{dz} = W\frac{dv}{dz} + \frac{1}{2}\rho_a C_d \nu^2 \pi D - \frac{Wg}{v} \tag{2}$$

$$\sigma = \frac{F}{A} = 3\eta\frac{dv}{dz} \tag{3}$$

$$\frac{dT}{dz} = -\frac{\pi D h(T - T_a)}{WC_p} \tag{4}$$

Here at any location z from the spinneret, W is the polymer mass flow rate, D, A, and ν are the diameter, the area of cross-section, and velocity of filament, F is the axial force experienced by the filament with contributions from inertia, air drag, and gravity, v is the cross-section area averaged instantaneous velocity, T is the melt temperature. Also the

polymer material properties are specified as: ρ is the density, η is the shear viscosity, C_p is the specific heat. Cooling air density, kinematic viscosity, and temperature are denoted by ρ_a, ν_a, and T_a respectively. The interaction of the filaments with the flow field surrounding it is taken into account through the drag and heat transfer coefficients without the detailed calculation of flow equations due to the complexities involved.

As the shear rate dependency of viscosity of PET at the take-up speeds analyzed in this article is expected to be small,[15] in accordance with the standard literature,[14] the rheological behavior of the melt is assumed to be Newtonian: stress is directly proportional to strain rate, the shear viscosity being the proportionality constant [eq. (3)]. The extensional viscosity is assumed to be three times the shear viscosity. The dependence of temperature on shear viscosity is assumed to be Arrehenius type with constant activation energy, E_a,

$$\eta = \eta_o \exp\left[\frac{E_a}{kT}\right] \tag{5}$$

where k is the Boltzmann constant. As we deal with POY spinning and freeze-point stress in the spinline remains below the critical stress (9.5 MPa)[16] for crystallization, the possible flow induced crystallization is negligible. Effect of surface tension and gravity are assumed to be negligible. The boundary conditions at the spinneret is

$$v = v_o; \quad T = T_0 \quad \text{at } z = 0 \tag{6}$$

and the boundary condition at the freeze point is

$$v = v_w; \quad T = T_g \quad \text{at } z = z_f \tag{7}$$

where T_0 is the polymer temperature in the spinneret, T_g is the glass transition of the polymer, and v_w is the take-up speed of the filament, and z_f corresponds to the location of the freezing point.

Drag coefficient (C_d) and heat transfer coefficient (h) are calculated as follows[14]:

$$h = 0.42\lambda_a \upsilon_a^{-0.334} D^{-0.666} v^{0.334} \left[1 + \left(\frac{8V_a}{\nu}\right)^2\right]^{0.167} \tag{8}$$

$$C_d = 0.37\ \mathrm{Re}_f^{-0.61} \tag{9}$$

where

$$\mathrm{Re}_f = \nu D/\upsilon_a \tag{10}$$

is the local Reynolds number. Here λ_a, υ_a, and V_a are the thermal conductivity, kinematic viscosity, and transverse velocity of the cooling air. In addition to the phenomena described earlier, the possible stress induced crystallization and associated effects on viscosity and heat release are ignored here as we concentrate on POY where the freeze-point stress levels are less than what is required for significant crystallization in the spinline.

In case of melt spinning with cross-flow quench (Fig. 1) with given spinneret capillary diameter ($D(z=0)$), polymer throughput W and temperature $T(z=0)$ and transverse cooling air velocity (V_a), the ordinary differential equations [eqs. (1)–(10)] can be solved as coupled initial value ($z = 0$) problem to march along z using Runge–Kutta algorithm. This exercise is carried out for several assumed values (following Newton – Raphson method of root finding) of axial force $F(z = 0)$ in polymer, until convergence is obtained when the position corresponding to the solidification temperature ($T = T_g$) matches the position corresponding to final take-up speed ($\nu = \nu_w$).

MODELING OF MELT SPINNING WITH AXIAL QUENCH

While Figure 1(a) shows the conventional melt spinning with cross-flow quench air cooling, Figure 1(b) shows the modification[12] of the quench air flow during melt spinning to achieve lower air drag and hence lower stress [eqs. (2) and (3)]. Here, the radially introduced quench air gets directed axially downwards along the filament. The co-current cooling air flow is accelerated parallel to the filament bundle by downstream reduction in the surrounding tube diameter. This flow pattern reduces the drag experienced by the polymer filaments, reducing the elongational stress, and any orientation induced crystallization.

The modification of quench air flow pattern surrounding the filament is achieved using a tube, which is composed of four different sections [Fig. 1(b)]. After a delay section 1, quench air is blown radially inward through finely perforated cylindrical section 2, enters almost axially into and is accelerated by a contraction section 3, and flows parallel to the filament through the long section 4 of reduced diameter, before venting out.

We represent the involved heat, mass, and momentum transport by the same eqs. (1)–(10) as employed for the cross-flow quenched system in the preceding section. The critical variation as compared to the cross-flow quench situation of Figure 1(a), from the modeling point of view, is the reduction in the heat transfer coefficient h according to eq. (8), as a single filament located at the center of the tube experiences no transverse air velocity ($V_a = 0$). More importantly, for the purpose of calculating h and C_d,

the filament velocity v in eqs. (8)–(10) is simply assumed to be replaced by the absolute relative velocity $|(v - V_{a,z})|$ of the filament compared to the axial quench air velocity, thus neglecting the possible effects associated with high absolute velocities of filament and quench air. Additionally, v^2 in the drag term in eq. (2) is replaced by $(v - V_{a,z})\ |(v - V_{a,z})|$. Also, this form takes care of situations where the air velocity exceeds the filament velocity (as we see later). These estimates are correct when cross-flow velocity (or corresponding Reynolds number) is much smaller than axial-flow velocity (or Reynolds number), which is precisely the case we analyze here. The axial quench velocity $V_{a,z}$ at each position (z) is assumed to be uniform across the tube cross-section, and is calculated applying the mass balance that all the air entering above that position (through part or whole of the perforated section 1) is flowing in axially downwards through the tube cross-section at that position:

$$\pi R_t^2(z) V_{a,z}(z) = \int_{z_1}^{z \le z_1 + z_2} 2\pi R_t(z_1 \le z \le z_1 + z_2) V_{a,y}(z_1 \le z \le z_1 + z_2) dz \tag{11}$$

where $R_t(z)$ refers to the tube diameter at location z, and $V_{a,y}(z)$ refers to radially inward velocity at the perforated walls of section 2 ($z = z_1$ to $z = z_1 + z_2$). Other than this, the procedure for computer simulation and obtaining convergence is the same as in the preceding section. Considering the high heat capacity of air (due large flow rate as compared to that of filament), the quench air temperature is considered to be unchanged at all z. Any small effect of change in cooling air density due to the small pressure changes along z is also neglected.

MATERIAL PROPERTIES

Simulations have been performed for PET, a widely used synthetic textile material. The following established relations[14] are used to estimate the material properties:

$$\text{Density: } \rho(z) = \rho_0 - \rho_1(T(z) - 273)$$
$$\text{Specificheat: } C_p(z) = C_{p0} + C_{p1}(T(z) - 273)$$

where $\rho_0 = 1356$ kg/m^3, $\rho_1 = 0.5$ kg/m^{3}K, and $C_{p0} = 1255$ J/kg K, $C_{p1} = 2510$ J/ kg K^2. Also the constants of eq. (5) used are $\eta_0 = 6.727 \times 10^{-4}$ kg/ms and $E_a/k = 6923.7$ K for viscosity estimations. The glass transition temperature (T_g) of PET is taken as 343 K.

RESULTS AND DISCUSSION

Conventional cross-flow quenched melt spinning

Stress at the point of solidification in the melt spinline is largely considered to determine the structure (such as chain orientation) and properties (such as residual drawability) of melt spun filaments, and therefore it is customary to characterize the melt spun filament based on this stress at the freeze point. The freeze-point stress itself is determined by the large number of melt spinning parameters, most important of them being the take-up speed as well as the quench air flow and temperature. The continuous lines in Figure 2 shows the calculated filament diameter, velocity, temperature, and stress profiles along the spinline during melt spinning with cross-flow quench at 0.85 m/s) (21°C) for polyester melt extrusion at 2.671 g/min at 290°C through circular capillary of diameter 0.33 mm while employing a take-up speed of 3270 m/min, to obtain filament of 8.17 dtex.

As seen in the plots, the polymer acceleration and filament attenuation are nearly completed at a distance of 0.35 m, when the temperature of the filament reaches T_g. As the quench air flows normal to the filament line, the axial velocity of the filament relative to the quench air, and hence the heat transfer coefficient increases monotonically until the freeze point. Though the spinline stress continues to increase beyond the freeze point, as discussed it is the stress at the freeze point that largely determines the filament structure and properties. This is shown further in Figure 3 (as dashed line) as increasing stress with filament cooling (as moving away from the spinneret), and the stress value at $T = T_g$ (vertical straight line) corresponds to the freeze-point stress.

Figure 4 shows the effect of increasing the quench air flow rate, while maintaining the same melt throughput and the spinning speed, for the quench flow case. At the higher quench air velocity, the faster cooling results in an earlier freeze point (earlier approach to final velocity) a somewhat higher velocity gradient, and a higher spinline stress. The continuous line in Figure 5 further shows this dependence of freeze-point stress on the quench velocity. Thus, from point of view of productivity, it is desired to have lower cross-flow quench air velocity for lower freeze-point stress while aiming higher drawability.

Axial-flow quenched melt spinning and comparison to cross-flow systems

Also included in Figure 2 are the spinline profiles with axial quench air flow [Fig. 1(b)] using the same polymer temperature through the same capillary,

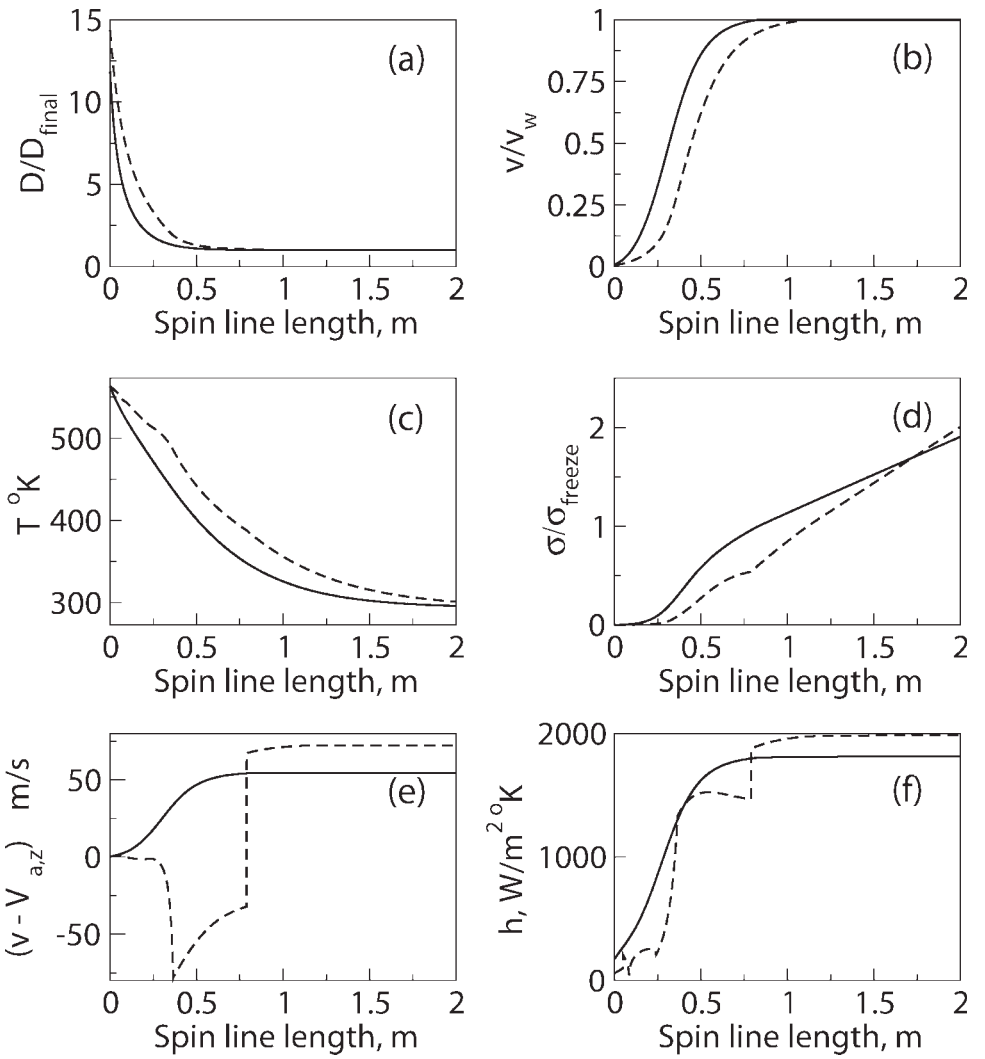

Figure 2 Comparison of filament (a) diameter/final diameter, (b) velocity/take-up speed, (c) temperature, (d) stress/freeze-point stress, (e) relative air velocity, (f) heat transfer coefficient for i) cross-flow quench system with take-up speed of 3270 m/min (continuous line) and ii) axial quench systems with take-up speed of 4330 m/min (dashed line).

while employing a radially inwards quench air speed of 1.11 m/s at the cylindrical screen-2 of diameter 95 mm and length 190 mm. As discussed with eq. (11), this allowed us to estimate the axial air velocity experienced by the filament. The take-up speed (4330 m/min) and melt throughput (3.54 g/min) are interrelated through the desired filament diameter, and were so chosen as to simulate producing the same 8.17 dtex filament with the same freeze-point stress (7.49×10^6 N/m^2) as for the cross-flow quenched melt spinning example described earlier. It shows that employing axial quench in place of cross-flow quench with the aforementioned parameters allows us increase the productivity from 3270 to 4330 m/min, or by 32%. This is further seen in Figure 3 for spinline stress plotted as function of reducing spinline temperature, where the stress at freeze point (at $T = T_g$) for axial flow

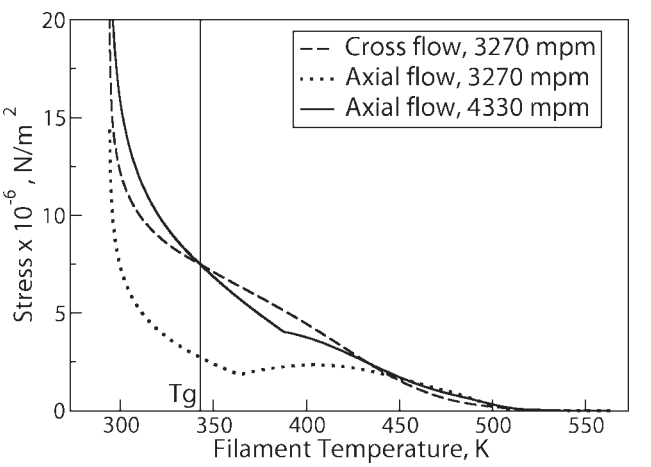

Figure 3 Spinline stress plotted as function of spinline temperature.

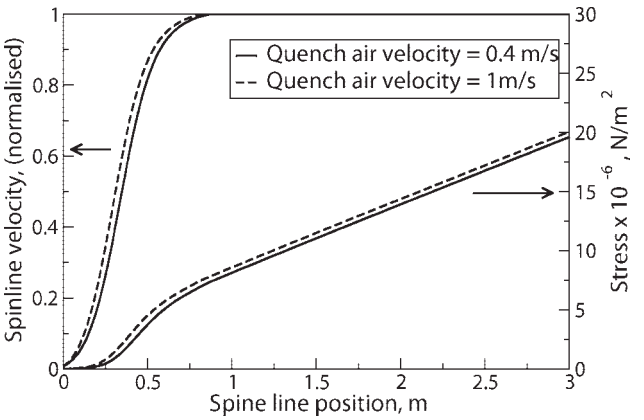

Figure 4 Effect of quench air velocity in cross-flow quenched melt spinning at take-up speed of 3270 m/min.

case at 4330 m/min matches that of cross-flow quench case at 3270 m/min. Dashed line in Figure 3 further shows that if the same diameter filament is produced at the speed of 3270 m/min, the corresponding freeze-point stress (at $T = T_g$) is reduced to about 1/3rd in case of axial quench air case as compared to the cross-flow quench case. Comparison of examples 1 and 3 of our reported experiments[13] indicate that such increase in productivity is indeed possible in industrial implementation employing multifilament melt spinning.

Comparison of the axial quench and cross-flow quench case profiles in Figure 2 shows that employing axial flow and constriction of the axial-flow tube results in acceleration and faster flow of quench air as compared to the filaments (negative relative velocity) in some parts of the spinline, thereby making negative drag contribution [eq. (2)] to the stress build up in the spinline. Additionally, the reduced velocity difference between the filament and the axially flowing quench air also reduces the heat transfer coefficient [eq. (8), Fig. 2(f)] and slows down the filament cooling (Fig. 2 (c), higher filament temperatures in axial-flow quench case). The overall impact of these factors in melt spinning with axial quench is to reduce the development of stress as compared to melt spinning with cross-flow quench, allowing higher speed to be employed in the former to match the same freeze-point stress.

Further to the slowed cooling of the filament seen for axial quench case along spinline as seen in Figure 2, it is also interesting to compare the time spent by the polymer in its melt state before solidification at $T = T_g$:

$$t_f = \int_0^{z_f} \frac{dz}{v} \tag{12}$$

This time is calculated from the simulations as 0.11 s and 0.2 s for cross-flow quench and axial-flow quench cases, respectively. The reduced spinline stress in case of the axial quench in spite of the higher take-up speed can thus also be seen as due to effective delay in filament cooling to solidification, as the filament diameter reduction (and thus the strain) is the same in both cases. Delayed quench, albeit by other means such as hot shroud around the spinneret, is a well known approach for reducing freeze-point stress in melt spinning lines.

While the profiles for cross-flow quench case are smooth, continuous, and monotonic, the air velocity and heat transfer coefficient for the axial flow case show sharp bends or discontinuity corresponding to sudden change in air acceleration corresponding to rate of change in cross-section of the tube at 0.24 and 0.365 m.

Figure 6 shows the profiles of filament velocity and spinline stress for axial-flow quench case at take-up speed of 3270 m/min at two different rates of axial quench air flow. Increasing the axial quench air rate results in an earlier approach to final velocity, as in the case of cross-flow quench (Fig. 4). However, in contrast to the intuition from a cross-flow quench (Fig. 4), the development of stress along the spinline is delayed in most parts of the spinline (Fig. 6) at the higher quench air rate in axial quench air flow case. This is because increasing the axial quench air flow rate allows the quench air velocity $V_{a,z}$ to approach/exceed the filament velocity earlier in the spinline, thus reducing the development of stress in the spinline. Figure 5 further shows this contrasting effect of 'air velocity' parameter on freeze-point stress in case of cross-flow and axial quench cases. The much coarser scale of the freeze-point stress axis for axial quench case in Figure 5 indicates that the effect of air flow is also much stronger in this case as compared to the cross-flow

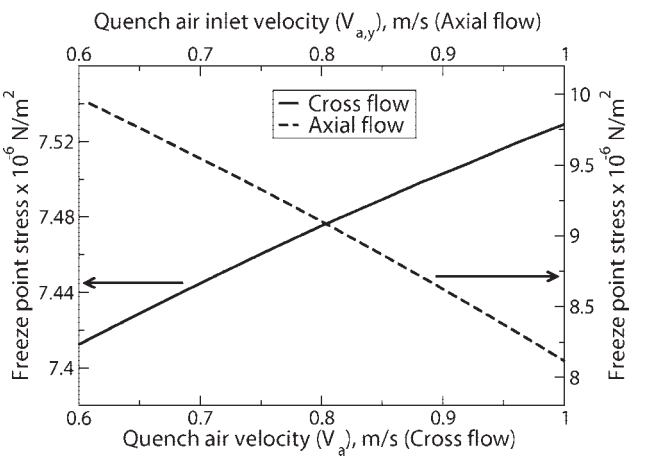

Figure 5 Contrasting effects of quench air velocity on freeze-point stress in cross flow (continuous line) at take-up speed of 3270 m/min and axial quenched (dashed line) melt spinning at take-up speed of 4330 m/min.

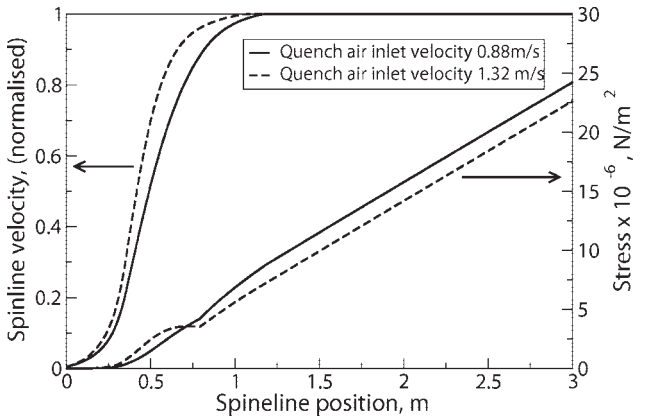

Figure 6 Effect of quench air flow velocity in axial air quenched melt spinning at take-up speed of 3270 m/min.

quench case. Thus, increasing the quench air flow in case of axial-flow quenched melt spinning case provides as a strong tool, for reducing the freeze-point stress and increasing drawability, or alternatively for increasing take-up speed for producing filaments of same properties such as freeze-point stress.

Following eq. (5), we had clarified that we had ignored flow induced crystallization (FIC) in view of the anticipated low values of stress in the spinline for POY spinning. To further ascertain that FIC is indeed negligible under the conditions employed in this work, we actually reproduced Figure 3 while modifying eqs. (4) and (5) according to the standard model of FIC.[14] We found that the modified figure was indistinguishable from the original figure. More rigorous models[17,18] for accounting FIC are now becoming available in the literature.

CONCLUSIONS

We have presented a simplified modeling approach for estimating quench air flow pattern during the axial quenched melt spinning of polymers. The numerical simulations and comparison with the conventional melt spinning with cross-flow quench shows that acceleration of axial quench air into a restricted diameter section co-current to filament reduces the heat transfer as well as the drag on the filament, thereby resulting in filaments with reduced freeze-point stress at equivalent take-up speed. Alternatively, higher take-up speed allowing higher productivity can be employed during melt spinning with axial quench while maintaining the same freeze-point stress and residual drawability. Quench air flow rate during axial air quenched melt spinning provides as a strong tool to manipulate filament properties such as freeze-point stress. Our simplified simulation approach allows us to demonstrate how increasing the quench flow rate during axial flow provides reduced orientation and higher residual drawability in the solidified filament.

References

1. Kumar, S.; Agrawal, A. K. Chem Fibers Int 2002, 52, 418.
2. Brody, H. J Appl Polym Sci 1986, 31, 2573.
3. MacLean, D. L.; Estes, R. T. U.S. Pat. 4,113,704 (1978).
4. MacLean, D. L.; Estes, R. T. U.S. Pat. 4,092,299 (1978).
5. Brody, H. Eur. Pat. 041,327 (1981).
6. Brody, H. U.S. Pat. 442,057 (1984).
7. Yoshimura, M.; Iohara, K.; Nagai, H.; Takahashi, T.; Koyama, K. J Macromol Sci 2003, 42, 189.
8. Yoshimura, M.; Iohara, K.; Nagai, H.; Takahashi, T.; Koyama, K. J Macromol Sci 2003, 42, 325.
9. Wandel, D.; Cziollek, J.; Thiele, U.; Klein, A.; Schumann, H.-D. U.S. Pat. 5,993,712 (1999).
10. Fochesato, A. Chem Fibers Int 2004, 54, 384.
11. Agarwal, U. S.; Asher, P.; Carr, W. W.; Pinaud, F.; Desai, P.; Abhiraman, A. S. Polymer Science and Fibre Science - Recent Advances; Fornes, R. E., Gilbert, R. D., Eds. VCH Pub. Inc.: New York, 1992; Chapter 5, pp 43–66.
12. Sweet, G. E.; Vassilatos, G. U.S. Pat. 5,824,248 (1998).
13. Agarwal, U. S.; Chatterjee, S.; Hebbar, P. Sumesh, P. T.; Mukhopadhyay, P.; Seth, K. K.; Aneja, A. P. World Patents WO/2009/024994 (2009).
14. Ziabicki, A.; Jarecki, L.; Wasiak, A. Comput Theor Polym Sci 1998, 8, 143.
15. Salem, D. R. Structure Formation in Polymeric Fibers; Hanser Gardner Publications: Cincinnati, Ohio, 2001.
16. Garg, S. J Appl Polym Sci 1984, 29, 2111.
17. Zheng, H.; Yu, W.; Zhang, H.; Zhou, C. Chin J Polym Sci 2006, 24, 1.
18. Doufas, A. K.; McHugh, A. J. J Rheol 2001, 45, 403.